Optics & Laser Technology 156 (2022) 108532

Contents lists available at ScienceDirect

Optics and Laser Technology

journal homepage: www.elsevier.com/locate/optlastec

Full length article

Ultrasensitive fiber-based gas pressure sensor based on harmonic Vernier effect with enhanced contrast

Chunhui Luo [a], Xiaoxu Chen [a], Shun Wu [a,b,*]

[a] Hubei Key Laboratory of Optical Information and Pattern Recognition, Wuhan Institute of Technology, Wuhan 430205, China
[b] State Key Laboratory of Transient Optics and Photonics, Xi'an Institute of Optics and Precision Mechanics, Chinese Academy of Sciences, Xi'an 710119, China

ARTICLE INFO

Keywords:
Harmonic Vernier effect
Fiber-based gas sensor
Fabry Perot Interferometer
Microstructure fiber

ABSTRACT

We propose and experimentally demonstrate a highly sensitive gas pressure sensor in parallel configuration based on harmonic Vernier effect. The sensor consists of two segments of 75 μm hollow-core capillaries as the sensing and reference Fabry Perot cavity. An open passage is formed by a 5 μm capillary in the sensing cavity while the reference cavity is sealed by a single-mode fiber. A pressure sensitivity of 279.52 pm/kPa is achieved. Our scheme uses "air" instead of "silica" reference cavity, which allows higher sensitivity for a given accuracy of cavity length control. In addition, we also developed a "superposition envelope" method, which improves the contrast by at least 3 dB for the Vernier envelope. This design for high-sensitivity optic fiber gas sensor can be a good candidate for ultrasensitive gas pressure applications.

1. Introduction

Fiber gas sensor has been widely researched in fields of gas pressure sensing [1–13] due to advantages of anti-electromagnetic interference capability, fast signal acquisition speed and compact structure [1].In recent years, a variety of gas pressure sensors based on different sensing mechanisms have emerged, including fiber grating sensors [2–4],anti-resonant waveguide sensors [5,6] and various types of fiber interferometers [1,7–10]. For pursuing high sensitivity, fiber-optic interferometer-based sensors are generally superior to fiber grating sensors and anti-resonant waveguide mechanism sensors. In particular, the sensitivity of fiber optic sensors that based on coating diaphragm are often tens of nm/kPa, or even higher [14,15]. However, they are usually difficult to obtain linear performance in addition to limited operation range.

Vernier effect is an effective way to achieve high sensitivity with large magnification using simple configurations. Various sensors based on Vernier effect are widely used in measuring pressure, temperature, stress, refractive index and many other fields [11–13,16–27]. It occurs when the Vernier condition ($n_2L_2 = jn_1L_1 + \Delta L$) is satisfied, where n and L represent the refractive index and the cavity length while the subscript 1 and 2 denotes for sensing FP and reference FP, respectively. ΔL is the detuning. The sensitivity of the envelope increases with j and inversely proportional to the detuning ratio, which is defined as $\Delta L/n_1L_1$ [12]. Most reported work is based on the fundamental Vernier effect, when the high sensitivity is achieved by a relatively small detuning ratio [16]. Nevertheless, a small detuning ratio results in a large free spectral range (FSR) of the envelope, which may impose difficulty in extracting the reference point of the envelope [17]. An alternate solution to high sensitivity is to use higher harmonics. The downside is that the contrast of the external envelope decreases with higher harmonics [12]. Ref. [13] proposed the "inner envelope" technique for determining the dip of the envelope. Ref. [17] further reported stress sensors with a third-order harmonic Vernier effect in 2019. This is by far the highest harmonic order realized experimentally. However, for gas sensors, it is more challenging to realize harmonic Vernier effect. The main reason is that the contrast of the Vernier envelope decreases as harmonics increases, and is further reduced by the open cavity configuration. In our previous work [12], we demonstrated a gas pressure sensor based on a cascading F-P structure for $j = 1$ and $j = 2$ Vernier effect. Both the sensing FPI and the reference FPI are a silica capillary with an air core diameter of 75 μm and 5 μm, respectively. The length of the sensing FPI is a few hundred microns. Although the sensitivity reported is the highest harmonic for gas sensor (80.8 pm/kPa) for the $j = 2$ case, to the best of our knowledge, we have shown that increasing the harmonic order results in the reduction of fringe contrast, imposing difficulty for extrapolating peaks of the envelope.

In this paper, we move a step forward and propose a scheme for a

* Corresponding author at: Hubei Key Laboratory of Optical Information and Pattern Recognition, Wuhan Institute of Technology, Wuhan 430205, China.
E-mail address: wushun@wit.edu.cn (S. Wu).

https://doi.org/10.1016/j.optlastec.2022.108532
Received 30 April 2022; Received in revised form 30 June 2022; Accepted 25 July 2022
Available online 3 August 2022

pressure sensor with improved sensitivity by over a factor of three compared to our previous work [12]. In addition to the "parallel-" instead of a cascaded-cavity configuration, we used "air" cavity to replace the previous "silica" reference cavity [12]. In principle, this would increase the sensitivity by about 1.5 times, given the same accuracy of cavity length control. Combined with the improved detuning ratio, we were able to achieve a high pressure sensitivity of 279.52 pm/kPa, which is 3.5 times higher than the previous work [12]. What's more, we developed a post-data processing method, called "superposition envelope", to improve the contrast of the envelope by >3 dB for high harmonic orders (j > 2).

2. Device fabrication and experiment principle

The proposed sensor has a parallel configuration as shown in Fig. 1. Both the sensing and reference cavity are formed by two separate segments of 75 μm capillaries. The reference cavity is end capped by a single mode fiber (SMF), while the sensing cavity is spliced to a 5 μm capillary acting as a gas inlet, as shown in Fig. 1(a and b).

The schematic diagram for the pressure test of the proposed sensor is shown in Fig. 1(c). Light from the broadband source (BBS, YSL, 900–1700 nm) reaches the sensing and reference cavities through a 2 × 2 fiber coupler. The reflected light from interfaces M1-M4 reaches the optical spectrum analyzer (OSA, YOKOGAWA AQ6370B). Both cavity lengths L1 and L2 are designed to meet the Vernier condition. The resulting reflection spectrum show periodic envelopes corresponding to different harmonics order *j*. During the test, the sensing cavity is enclosed in the vacuum chamber, while the reference cavity is exposed in air. The gas pressure inside the vacuum chamber can be controlled by the speedy valve and monitored by an electronic barometer (gauge: KJLC615TC, Kurt J. Lesker).

In order to obtain a clear Vernier reflection spectrum, there are a few key points to the design. Firstly, the lengths of the SMF fibers from the coupler to the two branches of the sensor are approximately equal, and much larger compared to the dimension of the sensor, which avoids causing additional interferences. Secondly, the intensities of the reflections from M1 and M3 are approximately equal to produce Vernier spectrum with good contrast. Thirdly, L_1 and L_2 are on the order of several hundred microns in order to reduce anti-resonance effect [28]. Fourthly, the capillary tube and the end-SMF fiber are made several centimeters long. The length is chosen such that the FSR of the cavity formed by the end fiber is less than the resolution of the spectrometer, which effectively reduces interference fringes from the end surfaces.

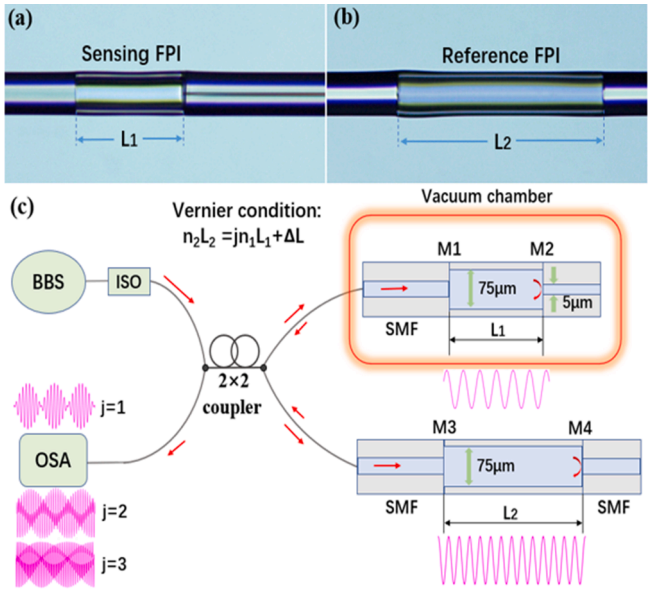

Fig. 1. (a and b) Side view microscopic pictures of the sensing and reference Fabry-Perot interferometer (FPI). (c) Schematic diagram for pressure test. Red arrows indicate the direction of light propagation. BBS: Broadband laser source, ISO: isolator, OSA: optical spectrum analyzer. (For interpretation of the references to colour in this figure legend, the reader is referred to the web version of this article.)

The reflected electric field of the three-beam interference can be express as:

$$E_r = E_0[\sqrt{R_1} + \sqrt{R_3} + (1-k_1)(1-\alpha_1)(1-R_1)\sqrt{R_2}e^{-j\phi_1} + (1-k_2)(1-\alpha_2)(1-R_3)\sqrt{R_4}e^{-j\phi_2}] \quad (1)$$

where $\phi_1 = 2\pi n_1 L_1/\lambda, \phi_2 = 2\pi n_2 L_2/\lambda$. In the above equation, E_0 is the electric field before the sensing and reference cavity; R_i is the reflectivity of M_i (i = 1,2…4); k_1 and k_2 are the losses of fusion splice at M1 and M3, respectively; α_1,α_2 are the transmission losses for the sensing and reference cavities, respectively. In this work, we ignore the change of refractive index of air under various pressures and consider R_i the same for i = 1,2...4, denoted by R. Therefore, the final reflective electric field can be simplified to:

$$E_r = E_0[A_1 + A_2 e^{-j\phi_1} + A_3\sqrt{R}e^{-j\phi_2}] \quad (2)$$

where $A_1 = 2\sqrt{R}, A_2 = (1-k_1)(1-\alpha_1)(1-R)\sqrt{R}, A_3 = (1-k_2)(1-\alpha_2)(1-R)\sqrt{R}$.

So the reflected light intensity can be expressed as:

$$I_r = (A_1^2 + A_2^2 + A_3^2 + I_1 + I_2 + I_3)I_0 \quad (3)$$

where $I_0 = E_0 * \overline{E}_0, I_1 = 2A_1A_2\cos(\phi_1), I_2 = 2A_1A_3\cos(\phi_2), I_3 = 2A_2A_3\cos(\phi_2 - \phi_1)$.

We explore the role of each term in Eq. (3), as shown in Fig. 2. I_1 and I_2 determine the shape of the Vernier envelope. I_3 contribute to the fringe contrast for envelope. We find two properties for the external and internal envelope, respectively, which can be used in the post-experiment data analyzation to improve the fringe contrast, especially for high harmonic orders. For external envelopes, the upper and lower envelope are in phase when the harmonic order *j* is odd, while out of phase when *j* is even. For example, in the case of *j* = 2, the upper envelope is π-shifted with respect to the lower envelope. For harmonic orders greater than one, there exist two sets of identical internal envelopes with π-shift to each other. For Internal envelopes exist only when *j* > 1, the upper and lower internal envelope are out of phase when *j* is odd, while in phase when *j* is even.

Reported work on harmonic Vernier effect usually chose the troughs of the external envelope as the point of interest for wavelength shift,

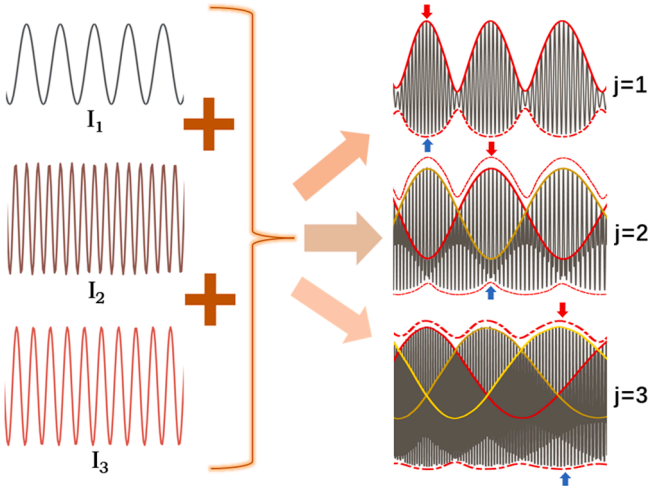

Fig. 2. Schematic diagram of theoretical simulation of Vernier effect.

rather than the peak of the external envelope [12,13,17]. This is because for high harmonics, the peak is much broader than the troughs due to low fringe contrast. Therefore, it is difficult to extrapolate the peak as reference point. Here, we propose a simple and effective "superposition envelope" method to improve the fringe contrast. By subtracting two in-phase envelopes, for example, the two internal envelopes for $j = 2$, we can construct a new envelope with the fringe contrast doubled. This is beneficial for determining an accurate reference point for wavelength shift measurements with enhanced linearity.

The magnification factor for the Vernier sensitivity is determined by the detuning ratio and the harmonic order j as follows [17]:

$$M = \frac{FSR_{env}}{FSR_2/j} = \frac{jn_1L_1}{jn_1L_1 - n_2L_2} = \frac{jn_1L_1}{-\Delta L} \quad (4)$$

So, the magnified sensitivity can be expressed as [17]:

$$S_{env} = M \times S_0 \quad (5)$$

where S_0 is the FPI sensitivity without the Vernier effect, which is reported to be 4.2 pm/kPa [12].

3. Experiment results

In order to investigate harmonics Vernier effect, we fabricated six samples, S1 to S6, with harmonics order j ranging from one to three. The pressure sensitivity for each samples were measured in a pressure range of 10–190 kPa. Table 1 lists the related dimension parameters and the sensitivity results for all samples. The length of the F-P cavity is chosen based on two considerations: sensitivity and compactness. The optimal value for the sensing cavity length is about 200–300 μm. Our experimental magnification factor M agrees well with the theoretical calculation in all cases.

The reflection spectrum for S2, S3 and S5 is shown in Fig. 3(a–c), corresponding to cases when the sensing cavity have a fixed length of 200 μm while j equals to 1, 2 and 3. As j increases from one to three, we found the sensor loss increases from 1.1 dB (S2) to 1.51 dB (S5). The loss ratio between the sensing to the reference cavity has an influence on the sensing performance. It determines the intensity ratio of the reflected light from both cavities, which further affects the contrast of the Vernier envelope in the interference spectrum. As j increases, the contrast of the external envelope decreases from 2.4 dB to 0.75 dB. By subtracting one of the dashed red envelopes from the other, we were able to construct a new envelope (solid red) with improved contrast, shown in Fig. 3(a–c). Fig. 3(d–f) represent the fast Fourier transformation (FFT) of the reflection spectra in Fig. 3(a–c). The calculated FSRs from the sensing and reference cavities matched the spatial frequencies of the FFT spectrum. The height difference between the two spatial frequency components also confirms that the intensity difference of the reflected light from both cavities becomes larger the as j increases.

Fig. 4(a–c) illustrate the contrast-enhanced envelopes of S2, S3 and S5 as the gas pressure increases from 10 kPa to 189 kPa. Fig. 4(d–f) plot the wavelength shift for the corresponding peaks and dips as a function of pressure. The linarities of the shift are all close to or above 99%. The direction of the wavelength shift was further verified in Fig. 5. When the detuning ΔL is negative ($jn_1L_1 < n_2L_2$), we can see that the troughs of the reflection spectra experience blue shift, as expected. In the case when ΔL is positive ($jn_1L_1 > n_2L_2$), the envelope experiences red shift. In this work, the highest sensitivity of 279.52 pm/kPa was achieved for sample S4. The reason why S4 ($j = 2$) had a higher sensitivity than S6 ($j = 3$) is because S4 has a much lower detuning ratio than that of S6 (Table 1), corresponding to a detuning of 6 μm for S4 and 17 μm for S6.

Fig. 6 illustrates the temperature performance of our sensor S2. We found the temperature sensitivity of 23.4 pm/°C with linearity of 99.3%. This corresponds to a temperature cross-sensitivity of 0.29 kPa/°C, which is a factor of 7.8 smaller than the result reported in Ref. [12]. This is because the materials for F-P cavities are different. In Ref. [12], the sensing cavity is made up of air while the reference cavity is a "silica" cavity. However, in this work, both cavities are "air" cavities. Since air has smaller thermal expansion coefficient than silica, our sensor is expected to have a lower temperature cross sensitivity than those who are consist of silica cavities.

Table 1
Configuration of different samples.

Sample	L_1 (μm)	L_2 (μm)	j	$\Delta L/(n_1L_1)$	$M^{(Cal)}$	$M^{(Exp)}$	$S_{env}^{(Exp)}$ (pm/kPa)
S1	294	280	1	5%	21	20.6	86.55
S2	200	212.5	1	5.63%	−16	−17.8	−74.6
S3	200	416.5	2	8.24%	−24.2	−24.3	−105
S4	200	394	2	3%	66.7	66.6	279.52
S5	200	617.5	3	8.64%	−34.3	−34.7	−159
S6	200	583	3	8.5%	35.3	35.4	148.75

4. Analysis and discussion

In our previous work, we have shown that increasing the harmonic order results in the reduction of fringe contrast, imposing difficulty for extrapolating peaks of the envelope. This is because as the harmonic order increases, one of the interference beams travels a longer distance before combined with the other interference beam, resulting in larger intensity difference between the two interference components. We summarized the contrast change for the external envelope in different harmonic cases in Fig. 7(a), and plotted the linearities for the corresponding sensitivities in Fig. 7(b). When j equals four, the contrast was too low to extrapolate an accurate trough wavelength. The corresponding reflection spectrum was not included in this work. In Fig. 7(a), we showed that the contrast of the external envelope decreased significantly as j increased, as shown for the red dots in Fig. 7(a). Our simulation (blue square) based on the above arguments agreed well with the experimental results. After we applied the "superposition envelope", the contrast was effectively enhanced by nearly 3 dB. Fig. 7(b) showed that linearity of the sensitivity was also improved by 1.2–3.3% for different j if we used the proposed "superposition envelope" method.

There are two modifications for the proposed configuration over the previous design [12]. One is that it utilizes "air" instead of "silica" as the reference cavity. The other is that we used parallel rather than cascading structure. Next, we shall discuss the advantages for the above two perspectives.

For the same optical path length, "air cavity" is longer than "silica cavity" due to the lower refractive index for air than silica. Therefore, for a given cavity length and cleaving accuracy, "air-air cavity" is capable of achieving a smaller detuning ratio than "air-silica cavity", and thus obtain a higher sensitivity. This is illustrated in Fig. 8(a). For a cleaving accuracy of 5 μm, the sensitivity is predicted to be 1.5 times higher for air-air than air-silica sensor. Considering the sensitivity dependence on harmonic numbers, given the same cavity length and cleaving accuracy, "air-air" sensor for $j = 2$ is expected to reach the same sensitivity with "air-silica" sensor when $j = 3$. Fig. 8(b) illustrates an additional advantage of air cavity. That is, under the same cavity length and cleaving uncertainty, the resulting detuning uncertainty is smaller for "air-air" than "air-silica" case. In other words, the "air-air" configuration is more tolerant for cleaving uncertainty. An additional benefit for air cavity is the low temperature cross sensitivity as compared to silica cavity.

Although the cascading cavity is small and compact, the parallel cavity configuration has advantages in two aspects. On one hand, the light intensities that reach the two FPs are approximately the same, resulting in larger contrast for the envelope of the interference spectrum. For comparison, Fig. 8(c) shows the contrast of the external envelope experimentally obtained for the two different structures under the same condition. We can see that the external envelope contrast of the "air-air" is about a factor of two higher than that of the "air-silica" case. On the other hand, from the fabrication point of view, the reported sensor in

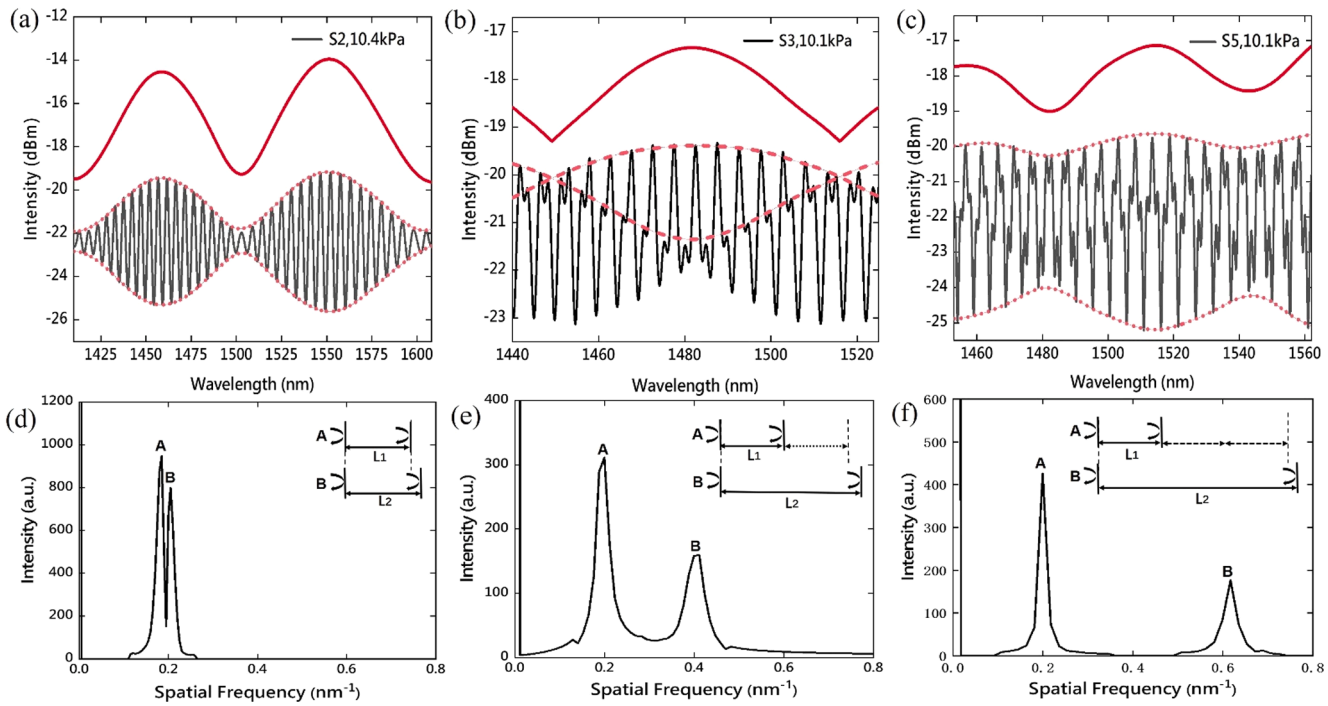

Fig. 3. The Vernier spectrum of (a) S2, (b) S3, and (c) S5. Black curves represent experimental reflection spectra. Red solid curves are calculated envelopes with enhanced contrast. The fast Fourier transformation (FFT) spectrum of (d) S2, (e) S3, and (f) S5. (For interpretation of the references to colour in this figure legend, the reader is referred to the web version of this article.)

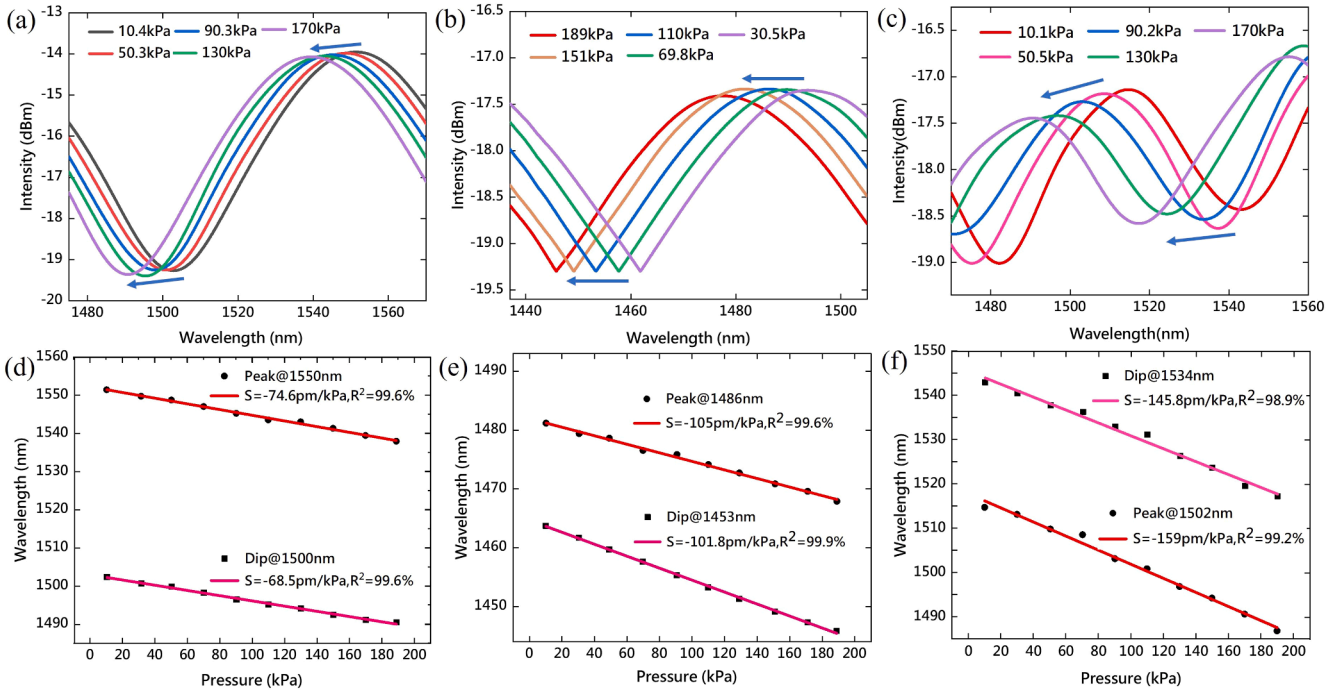

Fig. 4. Contrast-enhanced envelopes under various pressures for samples (a) S2, (b) S3, and (c) S5, respectively. Wavelength shift for peaks (red) and troughs (pink) for (d) S2, (f) S3, and (e) S5, respectively. S represents for the pressure sensitivity in each case. (For interpretation of the references to colour in this figure legend, the reader is referred to the web version of this article.)

this work is easier to fabricate than the cascading cavities [12]. This is because cascading FPs requires precise length control for both cavities. Whereas, for the parallel design, since both cavities are made at different times, the failure of making one cavity does not affect the fabrication of the second cavity.

5. Conclusions

We report a highly sensitive gas pressure sensor based on harmonic Vernier effect. The proposed configuration has two major improvements over the previous design [12]. By utilizing "air-cavity" as the reference cavity instead of "silica", smaller detuning ratio can be achieved given

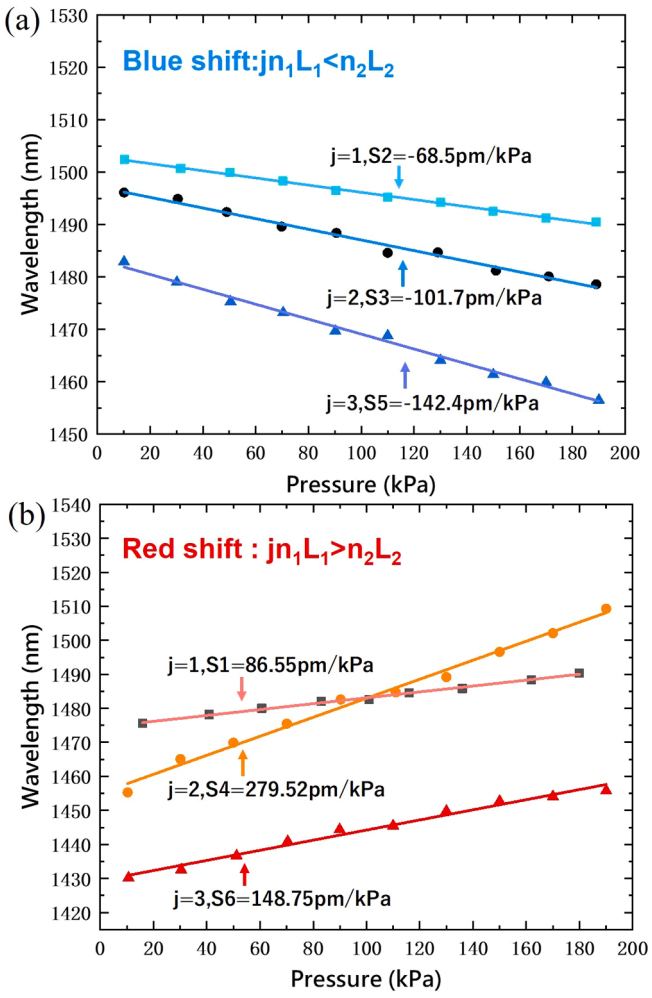

Fig. 5. Experimental verification for (a) blue shift and (b) red shift when the corresponding condition is satisfied. (For interpretation of the references to colour in this figure legend, the reader is referred to the web version of this article.)

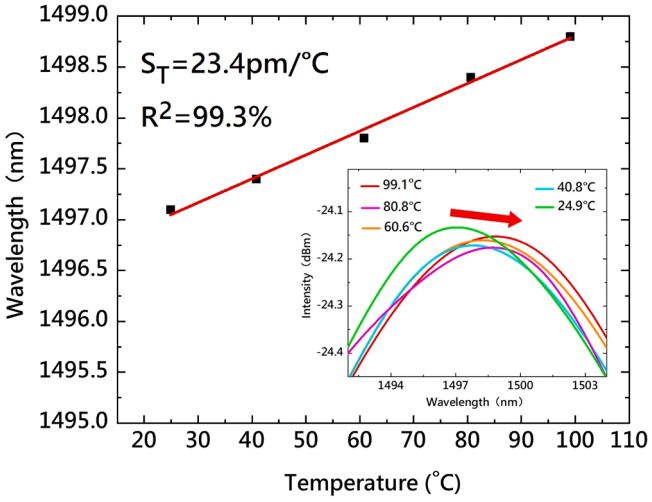

Fig. 6. The temperature performance of S2. Inset: The interference spectrum showing the wavelength of the interference peak shift as temperature increases.

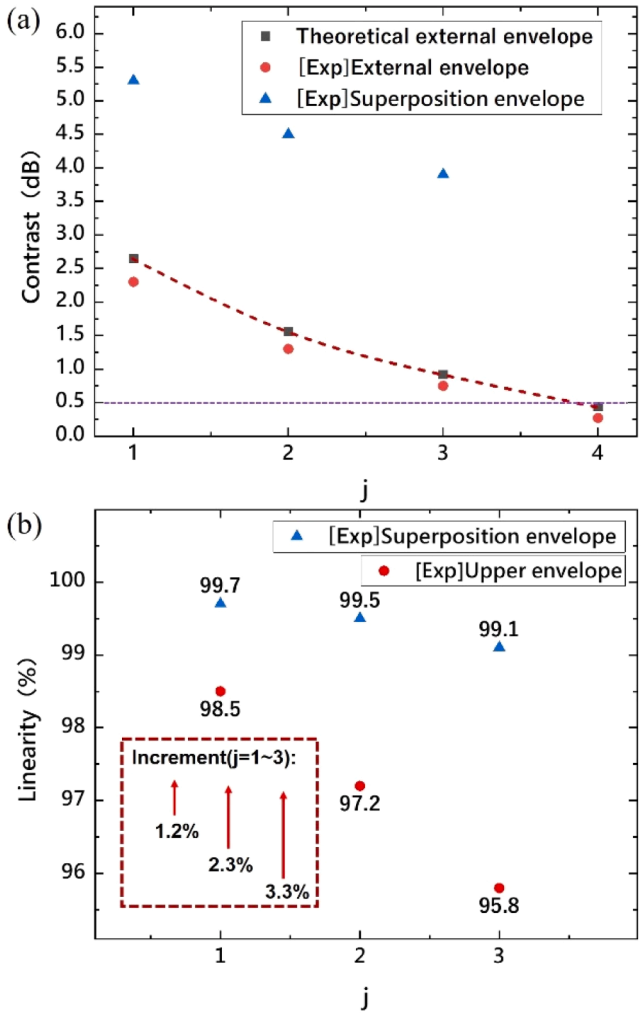

Fig. 7. (a) Comparison for the contrast of Vernier envelope: theoretical (black square), experimental (red dot) and enhanced contrast using the "superposition envelope" (blue triangle). (b) Comparison for the linearity of pressure sensitivity when the original envelope (red dot) and the extrapolated envelope (blue triangle) by the "superposition envelope" is used, respectively. (For interpretation of the references to colour in this figure legend, the reader is referred to the web version of this article.)

the same cavity length and fiber cleaving accuracy. The parallel cavity configuration ensures balanced light intensities for the two interference beams, promising a large contrast for the external envelope as compared to the cascading FP cavity configuration. In addition, we developed an effective data analyzation method named "superposition envelope" for extrapolating the external harmonic Vernier envelope with improved contrast by about 3 dB. This technique provides a solution to enhance the fringe contrast, which helps further increase the magnification values beyond the limit for the fundamental Vernier effect. We also experimentally demonstrate the proposed pressure sensor with a sensitivity of 279.52 pm/kPa, with the magnification factor of 67.7 and temperature cross sensitivity of 0.29 kPa/°C. In practical applications, a small detuning ratio is the key to obtain high sensitivity. However, fine-tuning of the interferometer optical path length can be quite challenging technically. Sensor based on higher-order harmonics with parallel FP configuration not only give higher sensitivity, but also allows better fabrication tolerances than that of the cascading configuration. This design with combined advantages of high sensitivity performance, low temperature cross sensitivity and ease of fabrication can be a good candidate for large-scale production of highly sensitive gas sensors in various areas such as medicine, biology and chemistry.

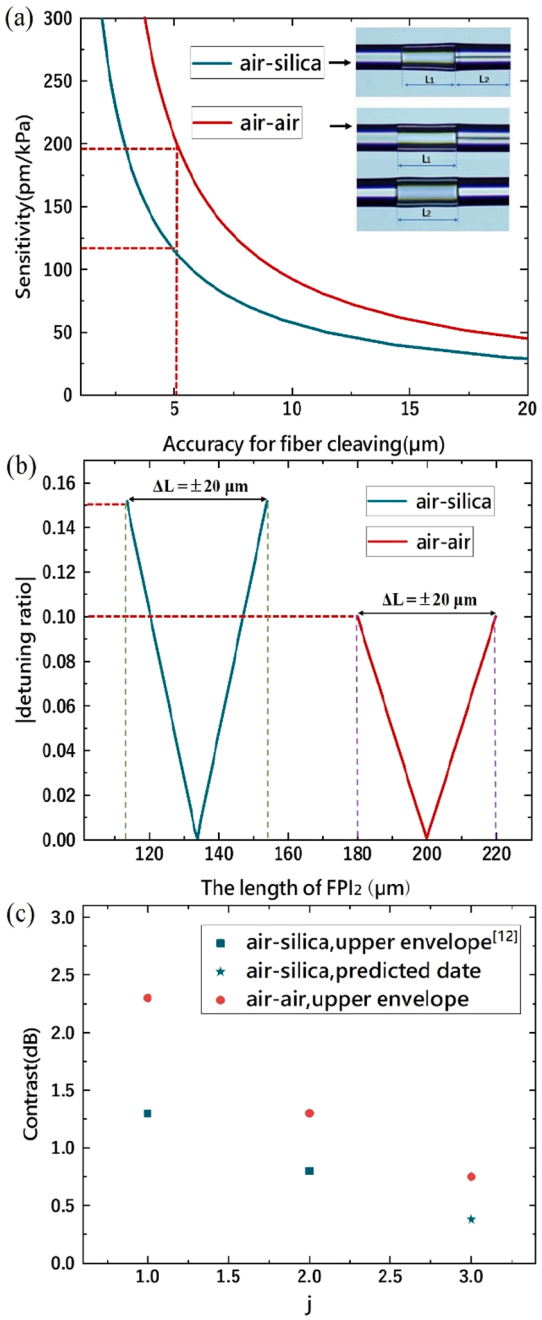

Fig. 8. Comparison for (a) the calculated sensitivity, (b) detuning ratio, and (c) contrast of the Vernier envelope when the reference cavity is air (red) or silica (black). The sensor cavity lengths in both cases are 200 μm. (For interpretation of the references to colour in this figure legend, the reader is referred to the web version of this article.)

CRediT authorship contribution statement

Chunhui Luo: Conceptualization, Methodology, Software, Formal analysis, Writing – original draft. **Xiaoxu Chen:** Software, Validation. **Shun Wu:** Data curation, Formal analysis, Writing – original draft, Writing – review & editing.

Declaration of Competing Interest

The authors declare that they have no known competing financial interests or personal relationships that could have appeared to influence the work reported in this paper.

Acknowledgments

This work is supported by grants from Campus Science Foundation of Wuhan Institute of Technology, China [22QD01], and Open Research Fund of State Key Laboratory of Transient Optics and Photonics [SKLST202105].

References

[1] C. Mao, B.o. Huang, Y. Wang, Y. Huang, L. Zhang, Y.u. Shao, Y. Wang, High-sensitivity gas pressure sensor based on hollow-core photonic bandgap fiber Mach-Zehnder interferometer, Opt. Exp. 26 (23) (2018) 30108.
[2] M. Smietana, W.J. Bock, P. Mikulic, J. Chen, Tuned pressure sensitivity of dual resonant long-period gratings written in boron co-doped optical fiber, J. Lightwave Technol. 30 (8) (2012) 1080–1084.
[3] X. Zhong, Y. Wang, C. Liao, S. Liu, J. Tang, Q. Wang, Temperature-insensitivity gas pressure sensor based on inflated long period fiber grating inscribed in photonic crystal fiber, Opt. Lett. 40 (8) (2015) 1791–1794.
[4] C.M. Jewart, Q. Wang, J. Canning, D. Grobnic, S.J. Mihailov, K.P. Chen, Ultrafast femtosecond-laser-induced fiber Bragg gratings in air-hole microstructured fibers for high-temperature pressure sensing, Opt. Lett. 35 (9) (2010) 1443.
[5] M. Hou, Y. Wang, Z. Feng, W. Ying, C. Liao, Gas pressure sensing based on antiresonant reflecting guidance hollow-core fiber, Optical Fiber Sensors Conference, 2017.
[6] Y.B. Yang, D.N. Wang, B. Xu, Z.K. Wang, Optical fiber tip interferometer gas pressure sensor based on anti-resonant reflecting guidance mechanism, Opt. Fiber Technol. 42 (2018) 11–17.
[7] Z. Li, C. Liao, Y. Wang, X. Lei, D. Wang, X. Dong, L. Shen, Q. Wang, K. Yang, J. Zhou, Highly-sensitive gas pressure sensor using twin-core fiber based in-line Mach-Zehnder interferometer, Opt. Exp. 23 (5) (2015) 6673–6678.
[8] R. Wang, X. Qiao, Gas refractometer based on optical fiber extrinsic Fabry—Perot interferometer with open cavity, IEEE Photon. Technol. Lett. 27 (3) (2015) 245–248.
[9] C. Li, J. Xiao, T. Guo, S. Fan, W. Jin, Interference characteristics in a Fabry–-Perot cavity with graphene membrane for optical fiber pressure sensors, Microsyst. Technol. 21 (11) (2015) 2297–2306.
[10] Z. Zhe, J. He, Q. Dong, Z. Bai, C. Liao, W. Ying, S. Liu, K. Guo, Y. Wang, Diaphragm-free gas-pressure sensor probe based on hollow-core photonic bandgap fiber, Opt. Lett. 43 (13) (2018) 3017–3020.
[11] P. Chen, X. Shu, H. Cao, High sensitivity refractive index sensor based on optical fiber ultra-weak Fabry-Perot interferometer, Lasers and Electro-Optics Pacific Rim, 2017.
[12] X. Yang, S. Wu, H. Cheng, J. Ma, S. Wang, S. Liu, P. Lu, Simplified highly-sensitive gas pressure sensor based on harmonic Vernier effect, Opt. Laser Technol. 140 (2021) 107007.
[13] Y. Yang, Y. Wang, J. Jiang, Y. Zhao, L. Li, High-sensitive all-fiber Fabry-Perot interferometer gas refractive index sensor based on lateral offset splicing and Vernier effect, Opt. – Int. J. Light Electron Opt. 196 (2019) 163181.
[14] X.u. Guo, J. Zhou, C. Du, X. Wang, Highly sensitive miniature all-silica fiber tip fabry-perot pressure sensor, IEEE Photon. Technol. Lett. 31 (9) (2019) 689–692.
[15] Y. Liu, Z. Jing, R. Li, Y. Zhang, Q. Liu, A. Li, C. Zhang, W. Peng, Miniature fiber-optic tip pressure sensor assembled by hydroxide catalysis bonding technology, Opt. Exp. 28 (2) (2020) 948.
[16] A.D. Gomes, H. Bartelt, O. Frazão, Optical Vernier effect: recent advances and developments, Laser Photon. Rev. 15 (7) (2021) 2000588.
[17] A.D. Gomes, M.S. Ferreira, J. Bierlich, J. Kobelke, O. Frazo, Optical harmonic Vernier effect: a new tool for high performance interferometric fibre sensors, Sensors 19 (24) (2019) 5431.
[18] P. Chen, Y. Dai, D. Zhang, X. Wen, M. Yang, Cascaded-cavity Fabry-Perot interferometric gas pressure sensor based on Vernier effect, Sensors 18 (11) (2018) 3677.
[19] Y. Zhao, H. Lin, C. Zhou, H. Deng, A.i. Zhou, L. Yuan, Cascaded Mach-Zehnder interferometers with vernier effect for gas pressure sensing, IEEE Photon. Technol. Lett. 31 (8) (2019) 591–594.
[20] Z. Li, Y.-X. Zhang, W.-G. Zhang, L.-X. Kong, T.-Y. Yan, P.-C. Geng, B. Wang, High-sensitivity gas pressure fabry-perot fiber probe with micro-channel based on Vernier effect, J. Lightwave Technol. 37 (14) (2019) 3444–3451.
[21] Q.H. Wang, X. Liu, D.N. Wang, Ultra-sensitive gas pressure sensor based on vernier effect with controllable amplification factor, Opt. Fiber Technol. 61 (2021) 102404.
[22] P. Zhang, M. Tang, F. Gao, B. Zhu, S. Fu, J. Ouyang, P.P. Shum, D. Liu, Cascaded fiber-optic Fabry-Perot interferometers with Vernier effect for highly sensitive measurement of axial strain and magnetic field, Opt. Exp. 22 (16) (2014) 19581.
[23] M. Quan, J. Tian, Y. Yao, Ultra-high sensitivity Fabry-Perot interferometer gas refractive index fiber sensor based on photonic crystal fiber and Vernier effect, Opt. Lett. 40 (21) (2015) 4891–4894.
[24] J. Zhang, H. Liao, P. Lu, X. Jiang, X. Fu, W. Ni, D. Liu, J. Zhang, Ultrasensitive temperature sensor with cascaded fiber optic fabry-perot interferometers based on Vernier effect, IEEE Photon. J. 10 (5) (2018) 1–11.
[25] T. Nan, B.o. Liu, Y. Wu, J. Wang, Y. Mao, L. Zhao, T. Sun, J. Wang, Ultrasensitive strain sensor based on Vernier- effect improved parallel structured fiber-optic Fabry-Perot interferometer, Opt. Exp. 27 (12) (2019) 17239.

[26] A.D. Gomes, J. Kobelke, J. Bierlich, J. Dellith, M. Rothhardt, H. Bartelt, O. Frazão, Giant refractometric sensitivity by combining extreme optical Vernier effect and modal interference, Sci. Rep. 10 (1) (2020).
[27] P.M.R. Robalinho, A.D. Gomes, O. Frazao, High enhancement strain sensor based on vernier effect using 2-fiber loop mirrors, IEEE Photon. Technol. Lett. 32 (18) (2020) 1139–1142.
[28] X. Zhang, H. Pan, H. Bai, Y. Ming, J. Wang, C. Deng, T. Wang, Transition of Fabry-Perot and antiresonant mechanisms via a SMF-capillary-SMF structure, Opt. Lett. 43 (10) (2018) 2268–2271.